Induction Heating During SiC Growth by PVT: Aspects of Axisymmetric Sinusoidal Modeling

Olaf KLEIN and Peter PHILIP

Abstract— **A model for the induction heating of an axisymmetric apparatus is presented, assuming sinusoidal time dependence. To ensure that the total current is equal in each ring of the induction coil, the decomposition of the total voltage into the ring voltages is determined by a linear system of complex equations. This method is then applied to simulate the heating process during the growth of SiC single crystals by the PVT method, where the electromagnetic problem is coupled to a transient heat equation. We compare results of the evolution of the heat sources as well as the resulting temperature field using the correct voltage distribution to the corresponding results using the simple homogeneous voltage distribution.**

Index Terms— **Electromagnetic heating, furnaces, modeling, semiconductor growth, simulation, voltage.**

I. Introduction

INDUCTION heating is used during many industrial processes such as metal hardening and forging (e.g. see [1], [2], and references therein). Induction heating is also used for the heating of crucibles during crystal growth, e.g. sublimation growth of silicon carbide (SiC) single crystals by physical vapor transport (PVT) (s. e.g. [3]). Even though in this article, we consider induction heating in the context of SiC growth by PVT, the induction heating model presented in Sec. II is also relevant to other applications, where the heated workpiece is axisymmetric and where the time dependence of the electromagnetic quantities is sinusoidal.

SiC is a semiconductor substrate material that is utilized in electronic and optoelectonic devices such as MESFETs, thyristors, LEDs, lasers, and sensors. An economically profitable use of SiC requires the availability of low-defect SiC boules with large diameter. In spite of substantial progress in recent years, the production process of low-defect SiC boules with large diameter remains challenging and an active research field in experimental work as well as modeling and simulation (s. e.g. [4], [5], [6], and references therein).

Large SiC boules are usually grown by the PVT method. Typically, modern PVT growth systems consist of a radio frequency (RF) induction-heated graphite crucible containing polycrystalline SiC source powder and a single-crystalline SiC seed (cf. Fig. 1). The source powder is placed in the hot zone of the growth apparatus, whereas the seed crystal is cooled by means of a blind hole, establishing a temperature difference between source and seed. At growth temperature, which can reach up to 3000 K for growth of the SiC polytype 6H, a low pressure argon (inert gas) atmosphere is established at some $2 \cdot 10^3$ Pa (cf. [7]). As the SiC source is kept at a higher temperature than the cooled SiC seed, sublimation is encouraged at the source and crystallization is encouraged at the seed, causing the partial pressures of species such as Si, Si_2C, and SiC_2 to be higher in the neighborhood of the source and lower in the neighborhood of the seed. As the system tries to equalize the partial pressures, source material is transported to the seed which grows into the reaction chamber.

The crystal's defect density and growth rate are strongly influenced by the temperature distribution, especially the temperature at the seed and the temperature difference between source and seed. Thus, the optimization of the temperature distribution with respect to favorable growth conditions is an important goal of apparatus design and control. However, due to the high temperatures, experimental verification of the correlation between the properties of the grown crystal, the temperature distribution, and external control parameters such as the coil position and the heating voltage is very intricate and costly. Thus, to assist the experimentalist, it is highly desirable to provide reliable numerical simulation tools based on a precise mathematical model. Recent papers concerned with modeling heat transfer during PVT growth include [5], [6], [8].

An accurate model of the heat transfer must include conduction through solid materials as well as through the gas phase, radiative heat transfer between surfaces of cavities, and the heat generated by induction heating. The induction heating model in an axisymmetric, sinusoidal setting is our main focus in this article.

Induction heating causes eddy currents in the conducting materials of the growth apparatus, resulting in heat sources due to the Joule effect. In the case of axisymmetry and sinusoidal time dependence, the heat sources can be computed using the coil ring voltages v_k as input data (cf. [9], [10], and Sec. II).

If the coil rings constitute the two-dimensional approximation of a single, connected coil, the total current in each coil ring must be the same. This is not reflected in the simple approximation by a homogeneous distribution of a total imposed voltage V to the rings, letting $v_k = V/N$, which we used to perform numerical simulations of induction heating in [11]. In our present article, to ensure identical total currents in the different rings, the amplitude of v_k and the phase shift between v_k and V are determined from a complex linear system (s. [12] and Sec. II). To the

This work was supported in part by the Bundesministerium für Bildung, Wissenschaft, Forschung und Technologie (German Ministry for Education, Science, Research, and Technology) (BMBF) within the program *Neue Mathematische Verfahren in Industrie und Dienstleistungen* (*New Mathematical Methods in Manufacturing and Service Industy*) # 03SP7FV16.

O. Klein and P. Philip are with the Weierstrass Institute for Applied Analysis and Stochastics (WIAS), 10117 Berlin, Germany (telephone: +49-30-20372-533, +49-30-20372-480, e-mail: klein@wias-berlin.de, philip@wias-berlin.de).

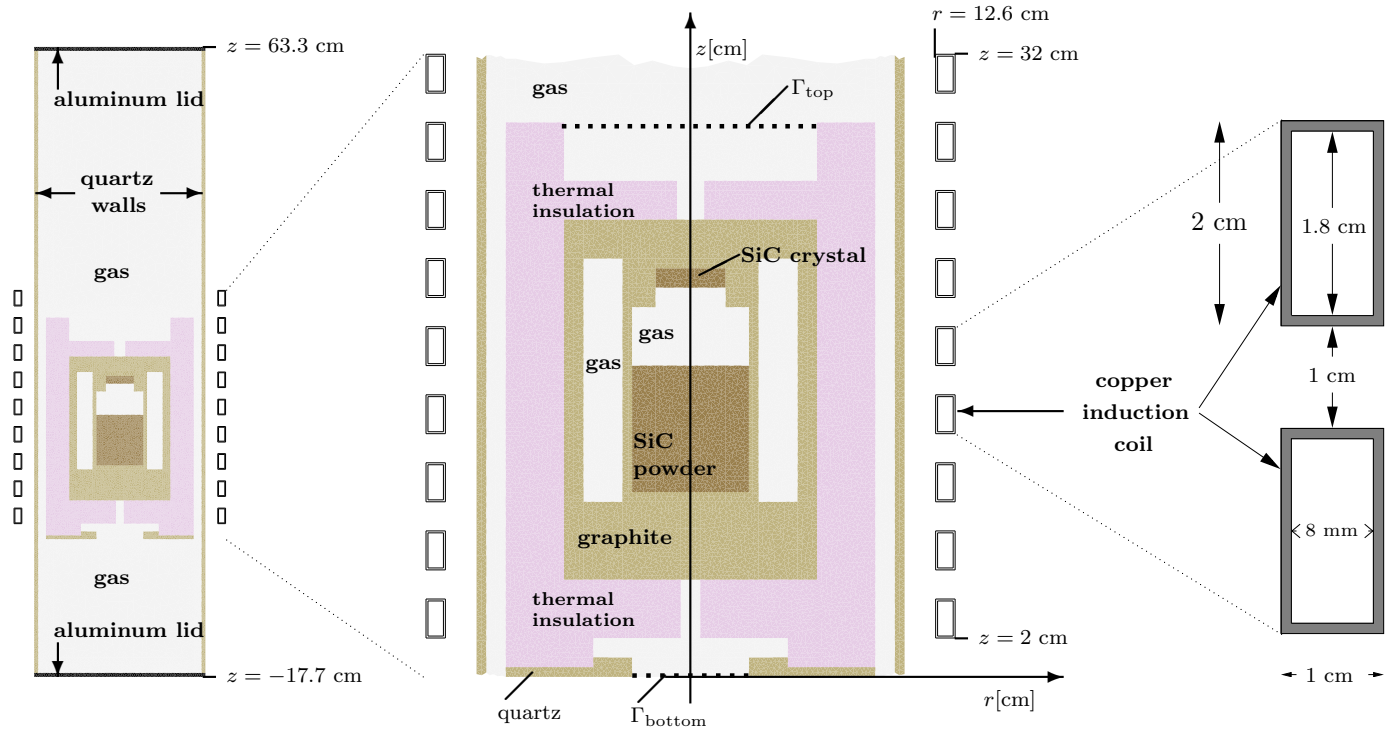

Fig. 1. Benchmark setup used for PVT growth at the Institute for Crystal Growth (IKZ), Berlin.

authors' knowledge, the subject of a correct voltage distribution to the coil rings has not received much attention in the literature. In [12], we used numerical simulations for a schematic growth apparatus to show that that one can gain up to 20 percent accuracy in the resulting heat sources by using the correct voltage distribution as compared to using an equal voltage in each coil ring.

In the present article we go one step further and compare the two methods, performing numerical simulations for the IKZ benchmark apparatus shown in Fig. 1, not only comparing the heat source distributions, but also the resulting temperature fields and their evolution. As explained above, the temperature fields are more relevant to the crystal growth process than the distributions of heat sources themselves.

II. Modeling Induction Heating

All solid materials in the growth system except quartz are considered as potential conductors, whereas quartz and the gas phase are treated as perfect insulators. We assume that displacement currents as well as surface currents can be neglected. Furthermore, we assume that a sinusoidal alternating voltage $V(t) = V_0 \sin(\omega t)$ is imposed in the coil, resulting in an alternating current that generates a rapidly oscillating magnetic field, inducing eddy currents in the conducting parts of the apparatus. The goal is to compute the distribution of heat sources in the apparatus caused by the eddy currents due to the Joule effect. To be able to consider the problem in an axisymmetric setting, the actual coil is replaced by N cylindrical rings with a sinusoidal alternating voltage imposed in each ring. All the involved electromagnetic quantities are assumed to be axisymmetric and sinusoidal. Thus, the voltage imposed in the k-th ring has the form $v_k(t) = \mathrm{Im}(\mathbf{v}_k e^{i\omega t})$, where i denotes the imaginary unit and $\mathbf{v}_1, \dots, \mathbf{v}_N$ are complex voltages satisfying

$$\sum_{k=1}^{N} \mathbf{v}_k = V_0. \tag{1}$$

Here, as in the following, we use the complex representation of sinusoidal functions, where bold face is used to denote complex representations.

The power density μ per volume of the heat sources can be computed from the current density $\mathbf{j}$:

$$\mu(r,z) = \frac{|\mathbf{j}(r,z)|^2}{2\,\sigma(r,z)}, \tag{2}$$

where (r,z) denote cylindrical coordinates, and σ denotes the electrical conductivity.

It is shown in [9], [10] that under the above assumptions, and given the total voltage in each coil ring $\mathbf{v}_k$, $k = 1, \dots, N$, there is a complex-valued magnetic scalar potential ϕ such that (cf. [10, Eq. (28)])

$$\mathbf{j} = \begin{cases} -i\omega\,\sigma\,\phi + \frac{\sigma\,\mathbf{v}_k}{2\pi r} & \text{in the } k\text{-th coil ring,} \\ -i\omega\,\sigma\,\phi & \text{in all other conducting materials.} \end{cases} \tag{3}$$

The potential ϕ is determined from the system of elliptic partial differential equations [10, (22), (29)], which we rewrite in the following divergence form (4) which is more suitable for our numerical approach via a finite volume discretization:

$$-\nu\,\mathrm{div}\,\frac{\mathrm{grad}(r\phi)}{r^2} = 0 \quad \text{in insulators,} \tag{4a}$$

$$-\nu \operatorname{div} \frac{\operatorname{grad}(r\phi)}{r^2} + \frac{i\,\omega\sigma\phi}{r} = \frac{\sigma\,\mathbf{v}_k}{2\pi r^2} \quad \text{in the } k\text{-th coil ring}, \tag{4b}$$

$$-\nu \operatorname{div} \frac{\operatorname{grad}(r\phi)}{r^2} + \frac{i\,\omega\sigma\phi}{r} = 0 \quad \text{in other conducting materials}, \tag{4c}$$

where ν denotes the magnetic reluctivity, i.e. the reciprocal of the magnetic permeability. The quantities ν and σ can vary in space, but they are supposed to be constant in time.

The system (4) is completed by interface and boundary conditions. Owing to the assumption of no surface currents, we have the interface condition [10, (30)]:

$$\begin{aligned} &\left(\frac{\nu\restriction_{\text{Material}_1}}{r^2}\operatorname{grad}(r\phi)\restriction_{\text{Material}_1}\right) \bullet \vec{n}_{\text{Material}_1} \\ &= \left(\frac{\nu\restriction_{\text{Material}_2}}{r^2}\operatorname{grad}(r\phi)\restriction_{\text{Material}_2}\right) \bullet \vec{n}_{\text{Material}_1} \end{aligned} \tag{5}$$

on interfaces between Material_1 and Material_2, where $\restriction$ denotes the restriction to the respective material, and $\vec{n}_{\text{Material}_1}$ denotes the outer unit normal vector to Material_1. It is also assumed that ϕ is continuous throughout the whole domain and that $\phi = 0$ both on the symmetry axis $r = 0$ and sufficiently far from the growth apparatus (cf. [5, Sec. 3.2]).

For each solution ϕ to (4), the corresponding total current in the k-th coil ring is given by

$$\mathbf{j}_k(\mathbf{v}_k, \phi) = \frac{\mathbf{v}_k}{2\pi}\int_{\Omega_k} \frac{\sigma}{r}\,\mathrm{d}r\mathrm{d}z \; - i\omega \int_{\Omega_k} \sigma\phi\,\mathrm{d}r\mathrm{d}z\,, \tag{6}$$

Ω_k denoting the two-dimensional domain of the k-th coil ring.

Since the coil rings constitute the approximation of a single, connected coil, the total current must be the same in each coil ring, i.e.

$$\mathbf{j}_k(\mathbf{v}_k, \phi) = \mathbf{j}_{k+1}(\mathbf{v}_{k+1}, \phi), \quad k \in \{1, \ldots, N-1\}. \tag{7}$$

Hence, the tuple $(\phi, \mathbf{v}_1, \ldots, \mathbf{v}_N)$ needs to satisfy the linear system consisting of (1) and (4) – (7). A method for the numerical solution of this system was described in [12, Sec. II.B]. Moreover, it was described in [12, Sec. II] how scaling of the solution $(\phi, \mathbf{v}_1, \ldots, \mathbf{v}_N)$ also allows to prescribe the total power.

III. Numerical Experiments

A. General Setting and Methods

The numerical simulations presented in the following were performed for the growth system displayed in Fig. 1, consisting of a container having a radius of 11 cm and a height of 81 cm placed inside of 9 hollow rectangular-shaped copper induction coil rings. It is assumed that all components of the growth system as well as all relevant physical quantities are cylindrically symmetric. As we are using the outer boundary condition $\phi = 0$, the domain where the problem for ϕ is solved has been chosen larger than the apparatus itself: $\phi = 0$ was set at $z = -0.8$ m, $z = 1.0$ m, $r = 1.2$ m, and $r = 1.0$ mm (to permit the evaluation of terms with r in the denominator). The dependence of ϕ on the domain size is investigated in [5].

The used heat transport model includes conduction through solid materials as well as through the gas phase and was described in [13], [14]. On the outside surfaces of the growth container, the temperature is fixed at room temperature $T_{\text{room}} = 293$ K, which agrees with experimental conditions [15]. Radiative contributions from the quartz wall and the Al lids are neglected. The inner container, consisting of the remaining solid components, is assumed to be exposed to a black body environment (e.g. a large isothermal room) radiating at room temperature T_{room}. This is reasonable, since the quartz walls are transparent. Thus, the outer boundaries of the inner container emit according to the Stefan-Boltzmann law. Radiative heat transfer between surfaces of cavities of the inner container is included using the net radiation method for diffuse-gray radiation as described in [13]. All solids are treated as opaque, except the SiC single crystal, where semi-transparency is accounted for via the band approximation model. For the two blind holes, we use black body phantom closures (denoted by Γ_{top} and Γ_{bottom} in Fig. 1) which emit radiation at T_{room}. Thus, we allow for radiative interactions between the open cavities and the ambient environment, including reflections at the cavity surfaces. The view factor algorithm is based on [16] and is described in [13, Sec. 4].

Assuming sinusoidal time dependence of the imposed alternating voltage, the heat sources are computed using the model described in Sec. II and using the numerical method described in [12, Sec. II.B]. The distribution of the heat sources is redetermined in each time step of the transient problem for the temperature evolution to account for temperature dependence of the electrical conductivity.

A finite volume method is used for the discretizations arising in the stationary computation of the magnetic scalar potential ϕ and in the transient temperature simulations. An implicit Euler scheme provides the time discretization of the temperature evolution equation; only emissivity terms are evaluated explicitly, i.e. using the temperature at the previous time step. The nonlinear systems arising from the finite volume discretization of the nonlinear heat transport problem are solved by Newton's method.

All simulations were performed using the software *WIAS-HiTNIHS*[1] which is based on the program package *pdelib* being developed at the Weierstrass Institute of Applied Analysis and Stochastics (WIAS), Berlin (cf. [17]).

As described in [13, Sec. 5], for simulations of the temperature distribution evolution, it is reasonable to assume that the gas phase is made up solely of argon, notwithstanding the fact that species such as Si, Si_2C, and SiC_2 make up a significant portion of the gas mixture at high temperatures.

The angular frequency used for the induction heating is $\omega = 2\pi f$, where $f = 10$ kHz, and the total voltage is $V_0 = V_{\text{eff}}\sqrt{2}$, where $V_{\text{eff}} = 330$V. In each material, the

[1] **Hi**gh **T**emperature **N**umerical **I**nduction **H**eating **S**imulator; pronounciation: ∼nice.

magnetic reluctivity is assumed to be $\nu = \mu_0^{-1} = \frac{10^7}{4\pi} \cdot \frac{\mathrm{Am}}{\mathrm{Vs}}$.

The material data used for argon, copper, graphite, insulation, SiC crystal, and SiC powder, respectively, are precisely the data provided in the appendices of [5] and [13], respectively. The only exception is the thermal conductivity of the SiC powder, which is according to [18, App. A]. The material data used for aluminum and quartz are provided in App. A.

B. Numerical Results and Discussion

We discuss the results of two transient numerical simulations of the temperature field evolution, both starting at $T_{\mathrm{room}} = 293$ K. To assess the error made when distributing the total voltage homogeneously to the coil rings as compared with determining the ring voltages according to Sec. II, for the computations of the heat source distributions, one simulation (subsequently called **Cor**) uses the correct voltages, where $(\phi, \mathbf{v}_1, \ldots, \mathbf{v}_N)$ is determined according to (1) and (4) – (7); and the other simulation (subsequently called **Hom**) uses $\mathbf{v}_k = V_0/N$ for each ring, i.e. using the homogeneous voltage distribution. In the following, the subscript "cor" is used to refer to quantities from simulation **Cor**, and the subscript "hom" is used to refer to quantities from simulation **Hom**. After $t = 3$h, both simulations have reached a quasi-stationary final state.

For both simulations **Cor** and **Hom**, the currents $\mathbf{j}_k$ are computed numerically according to (6), where the integrals are approximated by sums over finite volume elements. For **Hom** at times $t = 1$h and $t = 3$h, the results in Table I show that the current in each of the outer rings ($k = 1, 9$) is almost twice the current in the other rings. For **Cor**, the total currents were calculated to $\mathbf{j}_k = (31.6 - 567i)$ A at $t = 1$h and to $\mathbf{j}_k = (31.8 - 566i)$ A at $t = 3$h, respectively. The minor differences between $t = 1$h and $t = 3$h are due to the temperature dependence of the electrical conductivity.

Table II shows that in **Cor**, the voltages in the outermost rings deviate from the homogeneous value of 51.9 V by some 15 percent.

The total electrical power P_{el} computed during simulations **Cor** and **Hom** at $t = 1$h and at $t = 3$h, respectively, is provided in Table III, which also contains the information on how P_{el} is split between the heating power $P_{\mathrm{heat}}^{[\mathrm{app}]}$ in the apparatus and the heating power $P_{\mathrm{heat}}^{[\mathrm{coil}]}$ in the coil.

Fig. 2 depicts numerical results at $t = 1$h (column (1)) and at the quasi-stationary final state $t = 3$h (column (2)). Rows (a) and (b) show the heat source distributions (left halfs) and the temperatures distributions (right halfs) computed during simulations **Cor** and **Hom**, respectively; row (c) depicts the corresponding absolute errors, and row (d) depicts the corresponding relative errors.

In the insulation material, the isotherms lie very dense, producing the dark outer regions in the temperature fields depicted in rows (a) and (b) of Fig. 2. The same holds inside the SiC source powder at $t = 1$h, where the interior of the powder is still relatively cold and its thermal conductivity is low.

Fig. 2(d) shows that the relative error of the heat sources reaches up to 30 percent in the lower parts of the insulation. However, for the effect on the temperature distribution, the error in parts of large heat sources (i.e. the outer graphite, cf. Fig. 2(a),(b)) is more relevant. Comparing Fig. 2(a),(b) with Fig. 2(d) shows that the error is between 10 and 20 percent in regions where μ is maximal. Still, Fig. 2(d)(2) shows that the relative error in the temperature field is low at $t = 3$h, and even though the absolute error inside the growth chamber is considerable (Fig. 2(c)(2)), the qualitative differences in the stationary temperature distributions are minor (Figs 2(a)(2),(b)(2)).

The situation is different at $t = 1$h, where both the absolute and the relative error of the temperature are considerable inside the SiC source powder (Figs 2(c)(1),(d)(1)). This can be significant, as knowledge of the temperature of the source during the heating stage is important, e.g. for allowing enough time for baking out contaminants (cf. [18]).

IV. Conclusions

In two transient numerical simulations of the temperature evolution in an induction-heated PVT growth apparatus, we evaluated the error made when using a homogeneous voltage distribution in the coil rings as compared to determining the correct ring voltages from a linear system of equations, ensuring that the total current in each coil ring is identical. We found relative errors of the heat sources of up to 30 percent. While the relative errors of the temperatures were some two percent in the quasi-stationary distribution at $t = 3$h with only minor qualitative differences, one can gain almost 10 percent accuracy for the temperature distribution inside the SiC source at $t = 1$h, which can e.g. help to correctly gauge the time to allow for the contaminant bake-out phase during the heating process.

Appendix

I. Material Data

The material data used for argon, copper, graphite, insulation, SiC crystal, and SiC powder, respectively, are precisely the data provided in the appendices of [5] and [13], respectively. The only exception is the thermal conductivity of the SiC powder, which is according to [18, App. A]. The material data used for aluminum and quartz are provided below, where ρ denotes mass density, σ denotes electrical conductivity, κ denotes thermal conductivity, c_{sp} denotes specific heat, and ε denotes emissivity.

A. Aluminum

Since in the considered apparatus, the Al parts are not heated significantly, a constant value is taken for each of the following quantities, considering the respective quantity at room temperature.

The material parameters used for the Al lids are

$$\rho^{[\mathrm{Al}]}[T] = 2700\ \mathrm{kg/m^3}, \qquad \sigma^{[\mathrm{Al}]}[T] = 3.72 \cdot 10^7\ (\Omega\mathrm{m})^{-1},$$
$$\kappa^{[\mathrm{Al}]}[T] = 237\ \mathrm{W/(m\ K)}, \quad c_{\mathrm{sp}}^{[\mathrm{Al}]}[T] = 896\ \mathrm{J/(kg\ K)}.$$

TABLE I

TOTAL CURRENTS IN COIL RINGS (NUMBERED FROM TOP TO BOTTOM) COMPUTED DURING SIMULATION **Hom** AT $t = 1\text{h}$ AND AT $t = 3\text{h}$, RESPECTIVELY.

k		1	2	3	4	5	6	7	8	9
Hom, $t =$ 1h:	$\mathrm{Re}(\mathbf{j}_k)$[A]	28.1	22.9	32.6	38.0	38.9	35.9	29.5	19.6	25.7
Hom, $t =$ 1h:	$\mathrm{Im}(\mathbf{j}_k)$[A]	-919	-515	-478	-470	-469	-471	-479	-516	-926
Hom, $t =$ 3h:	$\mathrm{Re}(\mathbf{j}_k)$[A]	28.2	23.1	32.9	38.3	39.3	36.2	29.8	19.8	25.8
Hom, $t =$ 3h:	$\mathrm{Im}(\mathbf{j}_k)$[A]	-918	-514	-477	-469	-468	-470	-479	-516	-926

TABLE II

VOLTAGES IN COIL RINGS (NUMBERED FROM TOP TO BOTTOM) COMPUTED DURING SIMULATION **Cor** AT $t = 1\text{h}$ AND AT $t = 3\text{h}$, RESPECTIVELY.

k		1	2	3	4	5	6	7	8	9
Cor, $t =$ 1h:	$\mathrm{Re}(\mathbf{v}_k)$[V]	43.7	50.7	54.4	56.3	56.8	56.2	54.4	50.1	43.5
Cor, $t =$ 1h:	$\mathrm{Im}(\mathbf{v}_k)$[V]	0.389	0.128	-0.187	-0.407	-0.451	-0.307	-0.023	0.310	0.548
Cor, $t =$ 3h:	$\mathrm{Re}(\mathbf{v}_k)$[V]	43.7	50.7	54.4	56.3	56.8	56.2	54.3	50.6	43.5
Cor, $t =$ 3h:	$\mathrm{Im}(\mathbf{v}_k)$[V]	0.393	0.130	-0.188	-0.411	-0.455	-0.311	-0.024	0.312	0.553

TABLE III

TOTAL ELECTRICAL POWER P_{el} AND TOTAL POWERS OF HEAT SOURCES IN THE APPARATUS $P_{\mathrm{heat}}^{[\mathrm{app}]}$ AND IN THE COIL $P_{\mathrm{heat}}^{[\mathrm{coil}]}$ AS COMPUTED DURING SIMULATIONS **Cor** AND **Hom** AT $t = 1\text{h}$ AND AT $t = 3\text{h}$, RESPECTIVELY.

	$(1\text{h})_{\mathrm{cor}}$	$(1\text{h})_{\mathrm{hom}}$	$(3\text{h})_{\mathrm{cor}}$	$(3\text{h})_{\mathrm{hom}}$
P_{el} [kW]	7.37	7.03	7.42	7.09
$P_{\mathrm{heat}}^{[\mathrm{app}]}$ [kW]	6.28	5.88	6.34	5.94
$P_{\mathrm{heat}}^{[\mathrm{coil}]}$ [kW]	1.09	1.15	1.08	1.15

B. SiO_2 *(Quartz)*

The material parameters used for SiO_2 are

$$\rho^{[\mathrm{SiO_2}]}[T] = 2600\ \mathrm{kg/m^3}, \quad \sigma^{[\mathrm{SiO_2}]}[T] = 0.0,$$

$$\kappa^{[\mathrm{SiO_2}]}[T] = \Big(1.82 - 1.21\cdot 10^{-3}\ T/\mathrm{K} + 1.75\cdot 10^{-6}\ (T/\mathrm{K})^2\Big)\ \mathrm{W/(m\ K)},$$

$$c_{\mathrm{sp}}^{[\mathrm{SiO_2}]}[T] = \Big(932 + 0.2564\ T/\mathrm{K} - 2.403\cdot 10^{7}\ (T/\mathrm{K})^{-2}\Big)\ \mathrm{J/(kg\ K)},$$

$$\varepsilon^{[\mathrm{SiO_2}]}[T] = 0.82 + 3.5\ \cdot 10^{-5}\ T/\mathrm{K}.$$

REFERENCES

[1] S. Zinn and S.L. Semiatin, *Elements of Induction Heating: Design, Control, and Applications*, ASM International, Metals Park, Ohio, 1988.

[2] E.J. Davies, *Conduction and Induction Heating*, vol. 11 of *IEE Power Engineering*, Peter Peregrinus Ltd, London, 1990.

[3] A.O. Konstantinov, "Sublimation growth of SiC," chapter 8.2, pp. 170–203 in G.L. Harris, Ed., *Properties of Silicon Carbide*, no. 13 in EMIS Datareview Series. Institution of Electrical Engineers, INSPEC, London, 1995.

[4] St.G. Müller, R.C. Glass, H.M. Hobgood, V.F. Tsvetkov, M. Brady, D. Henshall, D. Malta, R. Singh, J. Palmour, and C.H. Carter Jr., "Progress in the industrial production of SiC substrates for semiconductor devices," *Mater. Sci. Eng. B*, vol. 80, no. 1–3, pp. 327–331, 2001.

[5] O. Klein and P. Philip, "Transient numerical investigation of induction heating during sublimation growth of silicon carbide single crystals," *J. Crystal Growth*, to appear.

[6] M. Pons, M. Anikin, K. Chourou, J.M. Dedulle, R. Madar, E. Blanquet, A. Pisch, C. Bernard, P. Grosse, C. Faure, G. Basset, and Y. Grange, "State of the art in the modelling of SiC sublimation growth," *Mater. Sci. Eng. B*, vol. 61-62, pp. 18–28, 1999.

[7] D.L. Barrett, J.P. McHugh, H.M. Hobgood, R.H. Hopkins, P.G. McMullin, R.C. Clarke, and W.J. Choyke, "Growth of large SiC single crystals," *J. Crystal Growth*, vol. 128, pp. 358–362, 1993.

[8] Q.-S. Chen, H. Zhang, and V. Prasad, "Heat transfer and kinetics of bulk growth of silicon carbide," *J. Crystal Growth*, vol. 230, no. 1–2, pp. 239–246, 2001.

[9] S. Clain, J. Rappaz, and M. Swierkosz, "Coupling between nonlinear Maxwell and heat equations for an induction heating problem: Modeling and numerical methods," pp. 163–171 in M. Krizek et al., Ed., *Finite element methods. 50 years of the Courant element.*, vol. 164 of *Lect. Notes Pure Appl. Math.*, New York, 1994. Marcel Dekker, Inc.

[10] J. Rappaz and M. Swierkosz, "Modelling in numerical simulation of electromagnetic heating," pp. 313–320 in *Modelling and optimization of distributed parameter systems (Warsaw, 1995)*, New York, 1996. Chapman & Hall.

[11] O. Klein and P. Philip, "Transient numerical investigation of induction heating during sublimation growth of silicon carbide single crystals," preprint no. 659, Weierstraß-Institut für Angewandte Analysis und Stochastik, Berlin, 2001. [5] is a revised version of this paper.

[12] O. Klein and P. Philip, "Correct voltage distribution for axisymmetric sinusoidal modeling of induction heating with prescribed current, voltage, or power," *IEEE Trans. Mag.*, vol. 38, no. 3, pp. 1519–1523, May 2002.

[13] O. Klein, P. Philip, J. Sprekels, and K. Wilmański, "Radiation- and convection-driven transient heat transfer during sublimation growth of silicon carbide single crystals," *J. Crystal Growth*, vol. 222, pp. 832–851, 2001.

[14] N. Bubner, O. Klein, P. Philip, J. Sprekels, and K. Wilmański, "A transient model for the sublimation growth of silicon carbide single crystals," *J. Crystal Growth*, vol. 205, pp. 294–304, 1999.

[15] K. Böttcher, D. Schulz, and D. Siche, Institut für Kristallzüchtung (IKZ), Berlin, 2002, private communication.

[16] F. Dupret, P. Nicodéme, Y. Ryckmans, P. Wouters, and M.J. Crochet, "Global modelling of heat transfer in crystal growth furnaces," *Intern. J. Heat Mass Transfer*, vol. 33, no. 9, pp. 1849–1871, 1990.

[17] J. Fuhrmann, Th. Koprucki, and H. Langmach, "pdelib: An open modular tool box for the numerical solution of partial differential equations. Design patterns," *Proceedings of the 14th GAMM Seminar on Concepts of Numerical Software, Kiel, January 23–25, 1998*, Kiel, Germany, 2001.

[18] O. Klein and P. Philip, "Transient temperature phenomena during sublimation growth of silicon carbide single crystals," preprint no. 755, Weierstraß-Institut für Angewandte Analysis und Stochastik, Berlin, 2002, submitted.

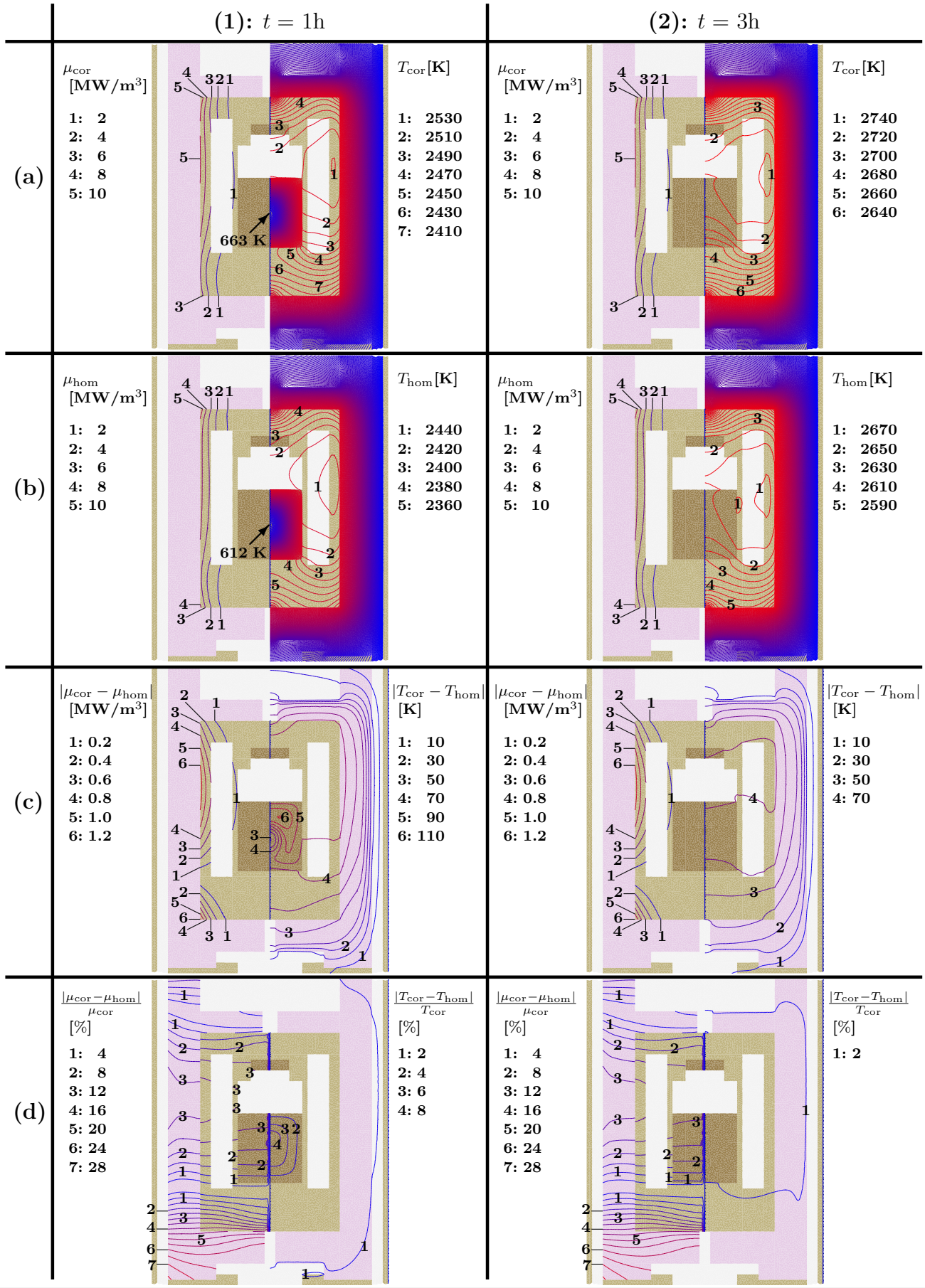

Fig. 2. Numerical results of computations of temperature distributions (right halfs) and heat source distributions (left halfs) at $t = 1$h (column (1)) and at the quasi-stationary final state $t = 3$h (column (2)). Rows: (a): using correct voltage distribution, (b): using homogeneous voltage distribution, (c): absolute error, (d): relative error.